

Lyapunov-based Switched Extremum Seeking for Photovoltaic Power Maximization

Scott J. Moura^{a,*}, Yiyao A. Chang^b

^a*Mechanical and Aerospace Engineering,
University of California, San Diego, CA 92093, USA*

^b*Scientific Research & Lead User Programs,
National Instruments, Austin TX 78759, USA*

Abstract

This paper presents a practical variation of extremum seeking (ES) that guarantees asymptotic convergence through a Lyapunov-based switching scheme (Lyap-ES). Traditional ES methods enter a limit cycle around the optimum. Lyap-ES converges to the optimum by exponentially decaying the perturbation signal once the system enters a neighborhood around the extremum. As a case study, we consider maximum power point tracking (MPPT) for photovoltaics. Simulation results demonstrate how Lyap-ES is self-optimizing in the presence of varying environmental conditions and produces greater energy conversion efficiencies than traditional MPPT methods. Experimentally measured environmental data is applied to investigate performance under realistic operating scenarios.

Keywords: Adaptive control; nonlinear control; Lyapunov methods; photovoltaic systems; renewable energy

1. Introduction

1.1. Problem Statement

Extremum seeking (ES) deals with regulating an unknown system to its optimal set-point. To this end, a periodic perturbation signal is typically

*Tel: +1-858-822-2406; Fax: +1-858-822-3107

Email addresses: smoura@ucsd.edu (Scott J. Moura), andy.chang@ni.com (Yiyao A. Chang)

used to probe the space. Once the optimal set-point has been identified, most methods enter a limit cycle around this point as opposed to converging to it exactly. Hence, one of the main challenges with ES is eliminating the limit cycle and converging to the optimal set-point asymptotically. This paper investigates a novel Lyapunov-based switched extremum seeking (Lyap-ES) approach that supplies asymptotic convergence to the optimal set-point. The proposed concept is demonstrated on a well-studied yet important problem: maximum power point tracking (MPPT) in photovoltaic (PV) systems.

1.2. Literature Review

Two bodies of literature form the foundation of this work: MPPT in PVs and extremum seeking control.

1.2.1. MPPT in PVs

The MPPT literature is extremely broad, and contains techniques that range in complexity, hardware, performance, and popularity, among other characteristics. The survey paper by Esham and Chapman [1] provides a comprehensive comparative analysis of over 90 publications on MPPT techniques. The most popular technique, perturb & observe (P&O), perturbs the input voltage to determine the direction of the maximum power point (MPP), and moves the operating point accordingly. However, the controller eventually enters a periodic orbit about the MPP. This approach does not require a priori knowledge of the PV system and is simple to implement. However, P&O can diverge from the MPP under certain variations in the environmental conditions [2], [3]. Recently, an exponentially decaying adaptive version of P&O has been developed [4], which has conceptual similarities to our proposed method. An alternative method, incremental conductance (IncCond), seeks to correct this issue by leveraging the fact that the slope of PV array power output is zero at the MPP. As a result, this algorithm estimates the slope of the power curve by incrementing the terminal voltage until the estimated slope oscillates about zero [5]. A drawback of P&O and IncCond methods is that both stabilize to limit cycles. Ideally, one desires a peak seeking scheme that is asymptotically convergent and self-optimizing with respect to shifts in the MPP. This motivates a control-theoretic approach to MPPT. A recent paper examined an adaptive backstepping approach, for which convergence to the MPP is theoretically proven under a persistency of excitation condition [6]. This paper examines an alternative non-model-based approach, extremum seeking.

Extremum seeking control and its application to photovoltaic systems represents an important and relevant subset of MPPT literature. Specifically, Leyva *et al.* [7] and Bratcu *et al.* [8] utilize extremum seeking for PVs by injecting an exogenous periodic signal. A separate research group developed ripple correlation control (RCC), which utilizes the signal ripple that inherently exists in systems with switching power electronics as the perturbation signal [9]. The stability and optimality of this approach has been established in [10]. RCC has the critical advantage of utilizing existing signal ripples, instead of injecting artificial perturbations. As such, RCC is only applicable to systems which inherently contain ripple characteristics. Recently, Brunton *et al.* [11] utilized the 120 Hz inverter ripple in a PV system within the context of an extremum seeking control theoretic approach to MPPT. Consequently this work established an important link between extremum seeking control and ripple-based MPPT [12].

1.2.2. Extremum Seeking Control Theory

Prior to the nonlinear and adaptive control theory developments in the 1970's and 1980's, extremum seeking was proposed as a method for identifying the optimum of an equilibrium map. Since then, researchers have extended extremum seeking to the general class of nonlinear dynamical plants (see e.g. [13], [14]) and applied the algorithm to a wide variety of applications (e.g. air flow control in fuel cells [15], wind turbine energy capture [16], ABS control, and bioreactors [17]). During this period there have been several innovations that have improved the practicability of ES. For example, convergence speed can be enhanced by adding dynamic compensators [18] or applying alternative periodic perturbation signals [19]. A Newton-based algorithm can also be developed by estimating the Hessian of the unknown nonlinear map [20].

1.3. Contributions

This study focuses on a general problem - asymptotic convergence to the extremum of a static nonlinear unknown function. As such, this paper extends the aforementioned research and builds on the authors' previous work [21] to add the following two new contributions to the ES control and MPPT bodies of literature. First, we introduce a switching method for ensuring asymptotic convergence to the optimal operating point, based on Lyapunov stability theory. Secondly, we demonstrate this algorithm in simulation for

MPPT problems in PV systems - a novel and control theoretic alternative to traditional MPPT methods.

1.4. Paper Outline

This paper is organized as follows: Section 2 describes the extremum seeking control design and our novel Lyapunov-based switching strategy. Section 3 discusses a case study of the proposed ES method on MPPT for PV systems. Finally, Section 4 presents the main conclusions.

2. Extremum Seeking Control

In this section we introduce and expand upon a simple yet widely studied extremum seeking (ES) scheme [13], [17] for static nonlinear maps, shown in Fig. 1. Since the case study on photovoltaic systems involves a static plant model (albeit parameterized by time-varying disturbances), the scope of our analysis is limited to static plants. One may also consider the more general singular perturbation analysis for dynamic plant models presented in [13].

Before embarking on a detailed discussion of this method, we give an intuitive explanation of how extremum seeking works, which can also be found in [13] and [17], but is presented here for completeness. Next, we design the Lyapunov-based switching extremum seeking control to eliminate limit cycles.

2.1. An Intuitive Explanation

The control scheme applies a period perturbation $a_0 \sin(\omega t)$ to the control signal \hat{u} , whose value estimates the optimal control input u^* . This control input passes through the unknown static nonlinearity $f(\hat{u} + a_0 \sin(\omega t))$ to produce a periodic output signal y . The high-pass filter $s/(s + \omega_h)$ then eliminates the DC components of y , and will be in or out of phase with the perturbation signal $a_0 \sin(\omega t)$ if \hat{u} is less than or greater than u^* , respectively. This property is important because when the signal $y - \eta$ is multiplied by the perturbation signal $\sin(\omega t)$, the resulting signal has a DC component greater than or less than zero if \hat{u} is less than or greater than u^* , respectively. This DC component is extracted by the low-pass filter $\omega_l/(s + \omega_l)$ and represents the sensitivity $(\frac{a_0^2}{2}) \frac{\partial f}{\partial u}(\hat{u})$. We may use a gradient update law $\dot{\hat{u}} = k(\frac{a_0^2}{2}) \frac{\partial f}{\partial u}(\hat{u})$ or a quasi-Newton method [22] to force \hat{u} to converge to u^* . Next we rigorously develop the ES algorithm.

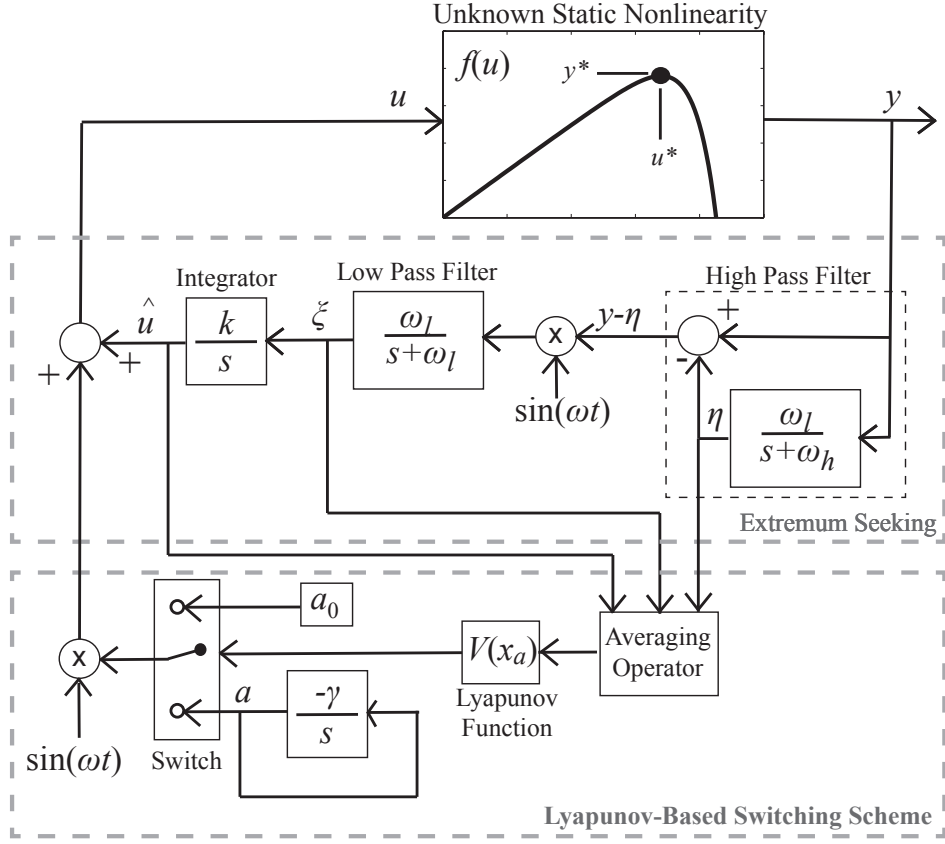


Figure 1: Block diagram of switched extremum seeking control system

2.2. Averaging Stability Analysis

Extremum seeking systems generally enter a limit cycle around the optimum, as opposed to converging to it asymptotically. To eliminate this drawback we propose a switching control scheme. This scheme decays the periodic perturbation's amplitude once the system has converged within the interior of a ball around the optimum. The switch criterion is determined using Lyapunov stability methods. Allowing the perturbation to decay exponentially is not new [4, 14], however it is the first application in a switched scheme, to the authors' knowledge.

In the following derivations, the Lyapunov function is ideally calculated with respect to a coordinate system centered at the extremum. However, the extremum is unknown *a priori*. In the case of MPPT for photovoltaics,

we assume knowledge of a “nominal” MPP, provided by the manufacturer under ideal conditions. The Lyapunov function will be evaluated with respect to a coordinate system centered at this nominal extremum. An analysis in Section 3.4 evaluates the impact of errors between the nominal and true extrema.

We start with a proof modified from Krstić and Wang [13], which uses averaging theory to approximate the ES system behavior, linearizes it about the equilibrium, and then shows the resulting Jacobian is Hurwitz. From this proof, our new contribution is to develop a Lyapunov function that senses proximity to the equilibrium point.

The state equations for the closed-loop ES system are:

$$\dot{\hat{u}} = k\xi \quad (1)$$

$$\dot{\xi} = -\omega_l \xi - \omega_l \eta \sin(\omega t) + \omega_l f(u) \sin(\omega t) \quad (2)$$

$$\dot{\eta} = -\omega_h \eta + \omega_h f(u) \quad (3)$$

$$u = \hat{u} + a_0 \sin(\omega t) \quad (4)$$

where each equation respectively represents the integrator, low-pass filter, high-pass filter, and perturbed control input. Now define a new coordinate system that shifts the nominal optimal operating point, denoted u^0 , to the origin

$$\tilde{u} = \hat{u} - u^0 \quad (5)$$

$$\tilde{\eta} = \eta - f(u^0) \quad (6)$$

resulting in the following translated system

$$\dot{\tilde{u}} = k\xi \quad (7)$$

$$\begin{aligned} \dot{\xi} = & -\omega_l \xi - \omega_l \tilde{\eta} \sin(\omega t) \\ & + \omega_l [f(\tilde{u} + u^0 + a_0 \sin(\omega t)) - f(u^0)] \end{aligned} \quad (8)$$

$$\dot{\tilde{\eta}} = -\omega_h \tilde{\eta} - \omega_h [f(\tilde{u} + u^0 + a_0 \sin(\omega t)) - f(u^0)] \quad (9)$$

Now we scale time $\tau = \omega t$.

$$\frac{d}{d\tau} \begin{bmatrix} \tilde{u} \\ \xi \\ \tilde{\eta} \end{bmatrix} = \delta \begin{bmatrix} K'\xi \\ -\omega'_L \xi - \omega'_L \tilde{\eta} \sin(\tau) + \omega'_L h(\tilde{u} + a_0 \sin \tau) \sin \tau \\ -\omega'_H \tilde{\eta} - \omega'_H h(\tilde{u} + a_0 \sin(\omega t)) \end{bmatrix}$$

where the parameters are normalized as follows:

$$k = \omega\delta K' = O(\omega\delta) \quad (10)$$

$$\omega_l = \omega\delta\omega'_L = O(\omega\delta) \quad (11)$$

$$\omega_h = \omega\delta\omega'_H = O(\omega\delta) \quad (12)$$

and K', ω'_L, ω'_H are $O(1)$ positive constants. The function $h(\theta) = f(u^0 + \theta) - f(u^0)$ satisfies the following properties in photovoltaic systems.

$$h(0) = 0 \quad (13)$$

$$h'(0) = f'(u^0) \quad (14)$$

$$h''(0) = f''(u^0) < 0 \quad (15)$$

$$h'''(0) = f'''(u^0) < 0 \quad (16)$$

These properties will be useful in our calculations later. Also note that (14) is equal to zero when the $u^0 = u^*$.

To investigate the stability properties of this system, we consider the averaged system - the standard approach for analyzing periodic systems. The averaged state variables are defined as follows [20].

$$x_a = \frac{1}{2\pi} \int_{\tau-2\pi}^{\tau} x(\sigma) d\sigma \quad (17)$$

where the period of the signal is 2π . Hence, our immediate goal is to use the notion of an averaged system to investigate the stability properties of the closed loop system. Applying the definition of averaging yields the following system

$$\frac{d}{d\tau} \begin{bmatrix} \tilde{u}_a \\ \xi_a \\ \tilde{\eta}_a \end{bmatrix} = \delta \begin{bmatrix} K' \xi_a \\ -\omega'_L \xi_a + \frac{\omega'_L}{2\pi} \int_0^{2\pi} h(\tilde{u}_a + a_0 \sin \sigma) \sin \sigma d\sigma \\ -\omega'_H \tilde{\eta}_a + \frac{\omega'_H}{2\pi} \int_0^{2\pi} h(\tilde{u}_a + a_0 \sin \sigma) d\sigma \end{bmatrix} \quad (18)$$

Now we must determine the equilibrium $(\tilde{u}_a^e, \xi_a^e, \tilde{\eta}_a^e)$ of this nonlinear system which satisfies:

$$0 = \begin{bmatrix} K' \xi_a^e \\ -\omega'_L \xi_a^e + \frac{\omega'_L}{2\pi} \int_0^{2\pi} h(\tilde{u}_a^e + a_0 \sin \sigma) \sin \sigma d\sigma \\ -\omega'_H \tilde{\eta}_a^e + \frac{\omega'_H}{2\pi} \int_0^{2\pi} h(\tilde{u}_a^e + a_0 \sin \sigma) d\sigma \end{bmatrix} \quad (19)$$

Let us postulate that \tilde{u}_a^e takes the form $\tilde{u}_a^e = b_1 a_0 + b_2 a_0^2 + O(a_0^3)$ and use a Maclaurin series expansion of $h(\tilde{u}_a^e + a_0 \sin \sigma)$. Following several algebraic calculations that use (13)-(16), one may show the equilibrium is given by:

$$\tilde{u}_a^e = b_0 - \frac{h'''(0)}{h''(0) + b_0 h'''(0)} a_0^2 + O(a_0^3) \quad (20)$$

where b_0 solves $h'''(0)b_0^2 + 4h''(0)b_0 + 2h'(0) = 0$.

$$\xi_a^e = 0 \quad (21)$$

$$\begin{aligned} \tilde{\eta}_a^e = & h'(0)b_0 + h''(0)b_0^2 + \frac{1}{6}h'''(0)b_0^3 + \left[h'(0)b_2 + \frac{1}{4}h''(0) \right. \\ & \left. + 2b_0b_2h''(0) + \frac{1}{4}b_0h'''(0) + \frac{1}{2}b_0^2b_2h'''(0) \right] a_0^2 + O(a_0^3) \end{aligned} \quad (22)$$

and $b_2 = -h'''(0)/(h''(0) + b_0h'''(0))$.

The Jacobian of (18) evaluated at $(\tilde{u}_a^e, \xi_a^e, \tilde{\eta}_a^e)$ is

$$J_a = \delta \begin{bmatrix} 0 & K' & 0 \\ \frac{\omega'_L}{2\pi} \int_0^{2\pi} h'(\tilde{u}_a^e + a_0 \sin \sigma) \sin \sigma d\sigma & -\omega'_L & 0 \\ \frac{\omega'_H}{2\pi} \int_0^{2\pi} h'(\tilde{u}_a^e + a_0 \sin \sigma) d\sigma & 0 & -\omega'_H \end{bmatrix} \quad (23)$$

Inspection reveals the Jacobian has a block-lower-triangular structure. As a result, J_a is Hurwitz if and only if

$$\int_0^{2\pi} h'(\tilde{u}_a^e + a_0 \sin \sigma) \sin \sigma d\sigma < 0 \quad (24)$$

We apply (13)-(16) to show that

$$\int_0^{2\pi} h'(\tilde{u}_a^e + a_0 \sin \sigma) \sin \sigma d\sigma = \pi h''(0)a_0 + O(a_0^2) \quad (25)$$

Using the property (15), we conclude the Jacobian is Hurwitz for sufficiently small a_0 . Since the Jacobian is Hurwitz, the averaged system is locally exponentially stable according to Theorem 4.7 of Khalil [23]. This also satisfies the conditions of Theorem 10.4 of Khalil [23], which states that the original system has a unique exponentially stable periodic orbit about $(\tilde{u}_a^e, \xi_a^e, \tilde{\eta}_a^e)$. Therefore the ES control system is stable in the sense that the averaged system converges exponentially for sufficiently small a_0 . We leverage this fact to design the Lyapunov-based switching criterion, described next.

2.3. Lyapunov-Based Switching Scheme

The Jacobian (23) approximates the system dynamics near the equilibrium $(\tilde{u}_a^e, \xi_a^e, \tilde{\eta}_a^e)$. We now use this Jacobian to develop a quadratic Lyapunov function for the switching control. First, we use (25) and similar calculations for $\int_0^{2\pi} h'(\tilde{u}_a^e + a_0 \sin \sigma) d\sigma$ to write the Jacobian as:

$$J_a = \delta \begin{bmatrix} 0 & K' & 0 \\ \frac{\omega'_L}{2} h''(0) a_0 & -\omega'_L & 0 \\ \omega'_H h'(0) & 0 & -\omega'_H \end{bmatrix} \quad (26)$$

where we use estimates for $h'(0)$ & $h''(0)$ which satisfy (14)-(15). Next we solve the following Lyapunov equation for P

$$PJ_a + J_a^T P = -Q \quad (27)$$

which has a unique solution under the conditions $Q = Q^T > 0$. This results in the following quadratic Lyapunov function

$$V(x_a) = \frac{1}{2} x_a^T P x_a \quad \text{where } x_a = [\tilde{u}_a \quad \xi_a \quad \tilde{\eta}_a]^T \quad (28)$$

which we use for the following switched control law:

$$u(t) = \begin{cases} \hat{u} + a_0 \sin(\omega t) & \text{if } V(x_a) > \varepsilon \\ \begin{cases} \hat{u} + a \sin(\omega t) \\ \frac{da(t)}{dt} = -\rho a(t), \quad a(0) = a_0 \end{cases} & \text{otherwise} \end{cases} \quad (29)$$

whose conditions are evaluated only when $\sin(\omega t)$ equals zero to ensure the control signal remains continuous in time.

Remark 1 (ES Re-engagement Property). The quadratic Lyapunov function in (28) estimates the averaged system's proximity to the equilibrium. That is, $V(x_a) \rightarrow 0$ as $x_a \rightarrow 0$. Once Lyap-ES converges sufficiently close to the optimum, the sinusoidal perturbation decays exponentially to zero and the control input arrives at u^* . If external disturbances cause the Lyapunov function value to increase above the threshold value ε , then the original amplitude a_0 is used until the system converges to the new extremum. Hence, the proposed switched control scheme is self-optimizing with respect to disturbances. This situation is illustrated in the case study on PV systems in Section 3.

Remark 2 (Positive Invariance Property). Note that the sub-level set $\Omega_c = \{x_a \in R^3 \mid V(x_a) \leq c\}$ which $V(x_a) \leq 0$ is positively invariant, meaning a solution starting in Ω_c remains in Ω_c for all $t \geq 0$. In other words, the Lyapunov function will be decreasing monotonically in time, therefore eliminating chattering behavior.

Remark 3 (Convergence Speed). During the case of constant perturbation amplitude, the convergence speed to the invariant set $\Omega_\varepsilon = \{x_a \in R^3 \mid V(x_a) \leq \varepsilon\}$ is characterized by the eigenvalues of (26). Once the perturbation amplitude switches to an exponential decay, the convergence is characterized by the decay parameter ρ in (29). In practice, one would use the algorithm parameters to compute convergence speeds from these relations.

Although we refrain from stating theorems and proofs in this paper, stability can be established by considering three points. First, the dynamics of a , which are in a cascade with the ES dynamics, are trivially stable. Second, $u(t)$ is continuous across the switching times since the conditions of (29) are evaluated only when $\sin(\omega t) = 0$. Given these two points, stability of the complete closed-loop system can be established by studying the ES dynamics augmented with the decaying amplitude state in (29). Unfortunately, the linearization test applied in [13] fails in this case because the Jacobian contains a zero eigenvalue. However, it may be possible to use an appropriately selected Lyapunov function or the Center Manifold Theorem (Section 8.1 of [23]) to prove local asymptotic stability.

3. Case Study: MPPT In Photovoltaic Systems

Next we examine the proposed Lyapunov-based switched extremum seeking scheme on the MPPT problem for PV systems. Solar energy represents a key opportunity for increasing the role of renewable energy in the electric grid. However, high manufacturing and installation costs have limited the economic viability of PV-based energy production [24]. Therefore, it is vitally important to maximize the energy conversion efficiency of PV arrays. This problem is particularly difficult because maximizing energy capture in PVs can depend on varying incident solar radiation, temperature, shading, system degradation, etc. As such, we desire control theoretic techniques that mathematically guarantee asymptotic convergence to the MPP, while rejecting disturbances due to changing environments.

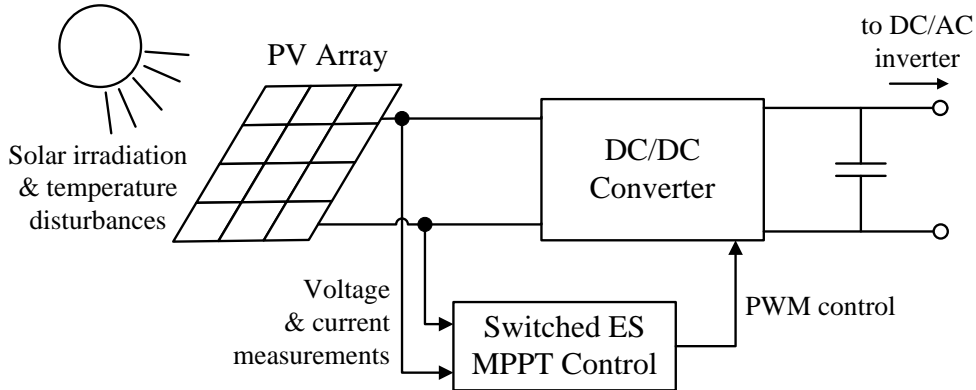


Figure 2: Photovoltaic (PV) system comprised of a PV array, DC/DC converter, and the proposed switched ES MPPT control algorithm

We consider a PV system comprised of a PV array, switching DC/DC boost converter, and the proposed Lyap-ES control algorithm, as depicted in Fig. 2. The DC/DC converter serves as the control actuator, which can impose various voltages across the PV array terminals. At the output-end of the converter, the voltage is fixed where it interfaces with the external system (e.g. DC/AC inverter and AC grid). To study this system we first summarize an established equivalent circuit model for PV arrays and a switching DC/DC boost converter model.

Next we apply Lyap-ES to the PV system and analyze the following: (i) The asymptotic convergence and self-optimizing behavior under external disturbances due to varying environmental effects, (ii) the algorithms merits and drawbacks versus traditional ES and MPPT algorithms, (iii) results from the application of experimentally measured transient solar irradiance and temperature data, and (iv) the impact of errors between the nominal and optimal MPP.

3.1. PV System Model Development

For the purposes of MPPT we consider an equivalent circuit model [25], [26] of a PV cell shown in Fig. 3. Within the PV control system literature, this model has been established as a sufficiently accurate representation of the physical system, for MPPT control design purposes [6, 25, 26, 27, 28, 29]. In particular, this model consists of an ideal current source I_{sc} in parallel with a diode and resistance R_p , all together in series with resistor R_s , which

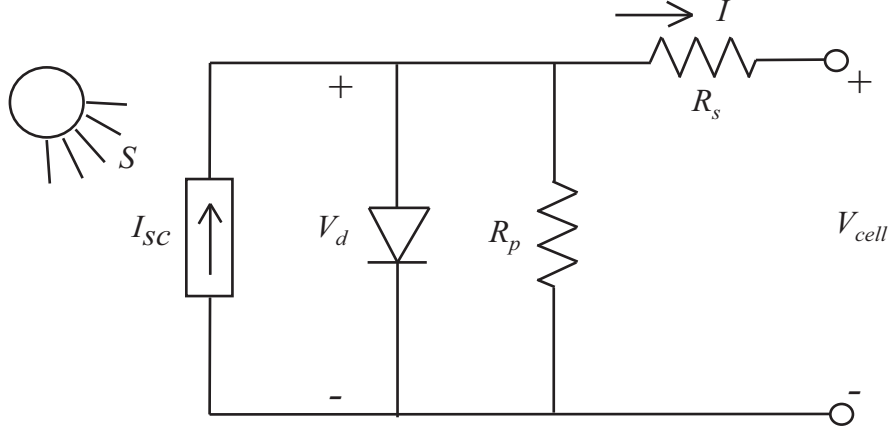


Figure 3: Equivalent circuit model of PV Cell [25], [26]

models contactor and semiconductor material resistance. The ideal current source delivers current in proportion to solar flux S , and is also a function of temperature T . The diode models the effects of the semiconductor material, and also depends on temperature. In total, the PV cell model equations are given by

$$V_d = V_{cell} + IR_s \quad (30)$$

$$I = I_{sc} - I_0 \left[\exp\left(\frac{qV_d}{AkT}\right) - 1 \right] - \frac{V_d}{R_p} \quad (31)$$

$$I_{sc} = [I_{sc,r} + k_I(T - T_r)] \frac{S}{1000} \quad (32)$$

$$I_0 = I_{0,r} \left(\frac{T}{T_r}\right)^3 \exp\left[\frac{qE_{Si}}{Ak} \left(\frac{1}{T_r} - \frac{1}{T}\right)\right] \quad (33)$$

$$V_{pv} = n_{cell} V_{cell} \quad (34)$$

The cell model is scaled to an array by considering n_{cell} cells in series (34). Parameters are adopted from [25].

The PV model is parameterized by environmental conditions - incident solar irradiation S and temperature T . Figure 4 demonstrates that current and power increase linearly with solar irradiation. Temperature has a more complex effect on current and power. The short circuit current increases with temperature, however the power decreases as temperature increases.

Consequently, PV cells operate best in full sunlight and cold temperatures. Our goal is to design a control loop that automatically tracks the MPP under changing environments.

A DC/DC boost converter steps up the PV array voltage and provides a control actuator for MPPT, via PWM on the switches. At the boost converter's output, a capacitor maintains a roughly constant voltage and is typically interfaced with the electric grid using a three-phase DC/AC inverter [2]. In this paper, we focus on the boost converter only for the purposes of MPPT, and assume the capacitor maintains a constant 120V at the output. In the following, we analyze the dynamics of a switching DC/DC boost converter model. Namely, we find the equilibrium of this system and show that it is locally exponentially stable. This analysis enables us to use the equilibrium as a reduced DC/DC model for the purposes of MPPT.

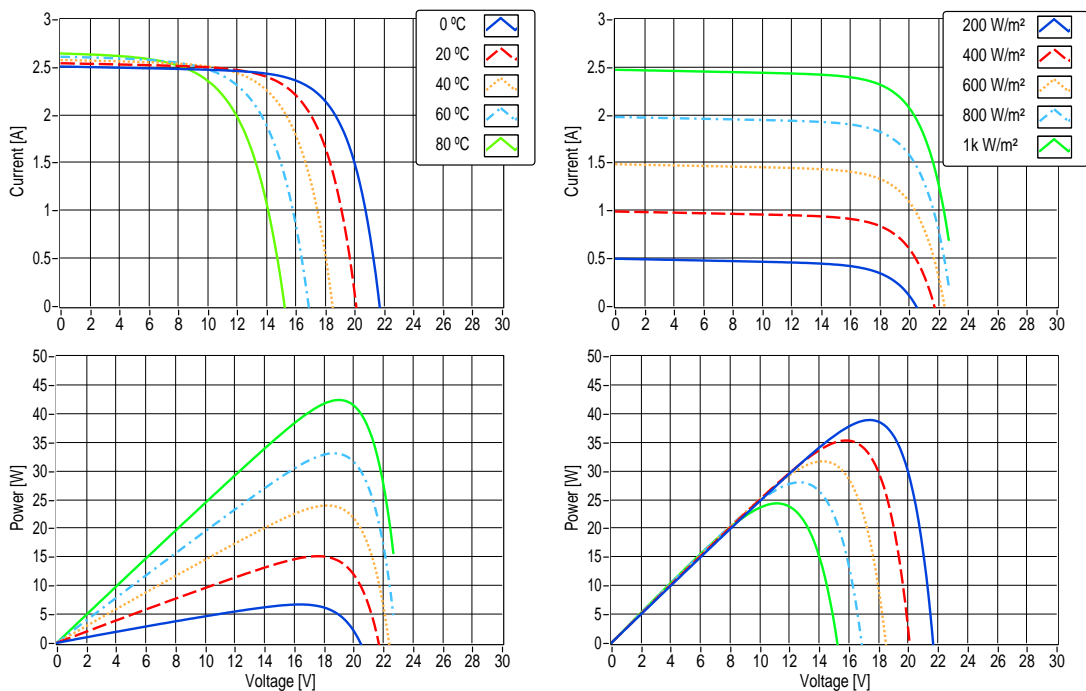


Figure 4: Characteristic I-V and P-V curves for varying T and $S = 1000 \text{ W/m}^2$ (left subplots), and varying S and $T = 25^\circ\text{C}$ (right subplots).

Figure 5 provides a schematic of a typical switching DC/DC boost converter. The input side interfaces with the PV array, represented by the static

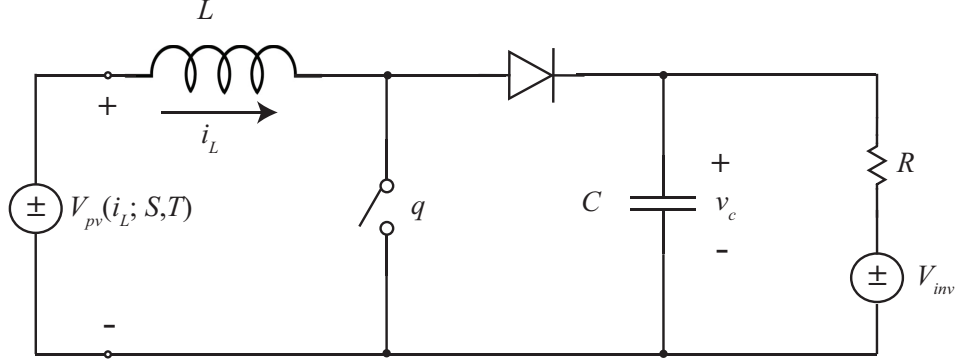


Figure 5: Circuit diagram of switching DC/DC boost converter model.

relation $V_{pv}(I; S, T)$ which verifies (30)-(34). The output side interfaces with a DC/AC inverter, which is modeled as a fixed voltage source V_{inv} and equivalent series resistance. The dynamics of this switched system, after applying the state-space averaging approach [30], are:

$$\frac{d}{dt}i_L = \frac{1}{L}V_{pv}(i_L; S, T) - \frac{1-d}{L}v_c \quad (35)$$

$$\frac{d}{dt}v_c = \frac{1-d}{C}i_L - \frac{1}{RC}(v_c - V_{inv}) \quad (36)$$

where $d \in (0, 1)$ is the duty ratio. The equilibrium for this nonlinear system (i_L^{eq}, v_c^{eq}) satisfies:

$$v_c^{eq} = (1-d)Ri_L^{eq} + V_{inv} \quad (37)$$

$$0 = V_{pv}(i_L^{eq}; S, T) - (1-d)^2Ri_L^{eq} - (1-d)V_{inv} \quad (38)$$

Now we analyze the stability of this equilibrium. First, we linearize (35)-(36) around (i_L^{eq}, v_c^{eq}) , producing the Jacobian

$$\begin{bmatrix} \frac{1}{L} \frac{\partial V_{pv}}{\partial i_L}(i_L^{eq}; S, T) & -(1-d)\frac{1}{L} \\ (1-d)\frac{1}{C} & -\frac{1}{RC} \end{bmatrix} \quad (39)$$

The eigenvalues λ of (39) satisfy the characteristic equation:

$$0 = \lambda^2 + \left[\frac{1}{RC} - \frac{1}{L} \frac{\partial V_{pv}}{\partial i_L}(i_L^{eq}; S, T) \right] \lambda - \frac{1}{RLC} \frac{\partial V_{pv}}{\partial i_L}(i_L^{eq}; S, T) + (1-d)^2 \frac{1}{LC} \quad (40)$$

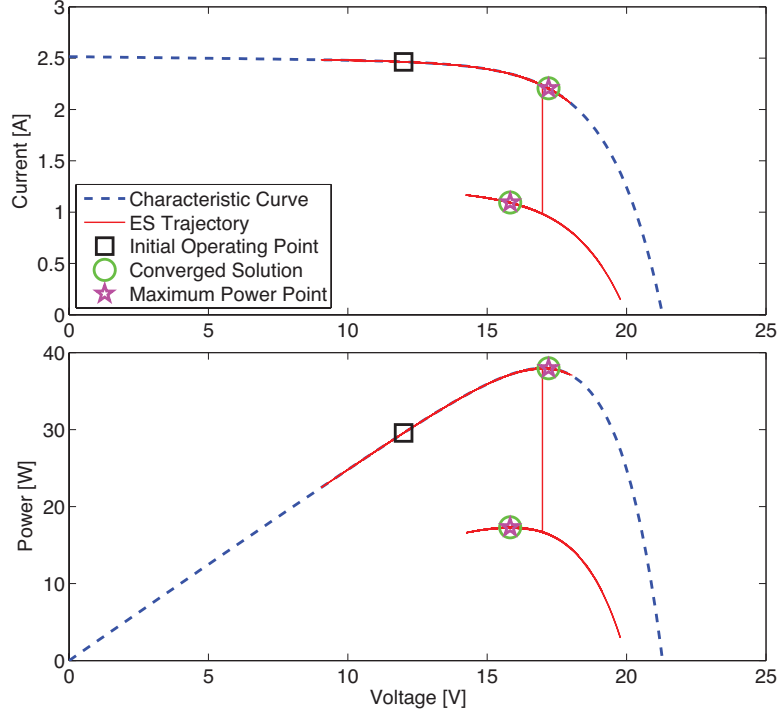


Figure 6: Trajectories of current and power on PV array characteristic curves for 1000 W/m^2 to 500 W/m^2 step change in solar irradiation.

Observe that $\partial V_{pv}/\partial i_L(i_L^{eq}; S, T) < 0$ over its entire domain, for all physically meaningful values of S, T . Therefore, all the coefficients of λ in (40) are positive. By the Routh-Hurwitz stability criterion, $\text{Re}[\lambda] < 0$. Consequently, the equilibrium (i_L^{eq}, v_c^{eq}) is locally exponentially stable.

For the proposed MPPT algorithm, we impose the condition that the switching converter dynamics are notably faster than the Lyap-ES loop dynamics. This enables us to use the stable equilibrium to model the DC/DC boost converter dynamics as:

$$0 = V_{pv}(I; S, T) - (1 - d)^2 RI - (1 - d)V_{inv} \quad (41)$$

where V_{pv} is the PV array voltage, V_{inv} is the constant 120V DC/AC inverter voltage, and d is the duty ratio control input.

3.2. Concept Demonstration

In this section we demonstrate Lyap-ES by (i) analyzing the impact of varying environmental conditions, and (ii) comparing it to P&O and traditional ES methods. In the first part we impose 1000 W/m^2 of solar irradiation and then provide a 500 W/m^2 step change at 200 ms. This might model the transient effect of a passing cloud blocking incident sunlight. The duty ratio is initialized at 0.9. The control parameters for Lyap-ES are provided in Table 1. Remarks on control parameter selection are included in Appendix A.

3.2.1. Impact of Varying Environmental Conditions

Figure 6 demonstrates the current and power trajectories superimposed on the PV array's characteristic I-V and P-V curves ($S = 1000 \text{ W/m}^2$). Lyap-ES indeed achieves the maximum power of 38W at voltage and current values of 17V and 2.24A for $S = 1000 \text{ W/m}^2$, and maximum power of 17.3W at voltage and current values of 18V and 1.09A for $S = 500 \text{ W/m}^2$. Moreover, one can see how the operating point jumps from the 1000 W/m^2 characteristic curve to the 500 W/m^2 curve during the step change. Immediately after the step change, the operating point is no longer at the MPP. The algorithm senses this change and reengages the perturbation to find the new MPP.

Time responses of power, duty ratio, and Lyapunov function value are provided in Figure 7. This figure demonstrates how Lyap-ES injects sinusoidal perturbations into the duty ratio to determine the MPP $u^* = 0.859$ for $S = 1000 \text{ W/m}^2$ and 0.868 for $S = 500 \text{ W/m}^2$. Note the perturbations begin to decay exponentially at 7.5 ms and $u(t)$ converges to u^* . Once the irradiation changes at 200 ms, the perturbation re-engages to search for the new MPP. Once it converges sufficiently close to the optimal duty ratio, the perturbation amplitude decays exponentially once again.

The switch behavior can be understood by analyzing Figure 7. At 7.5 ms, $V(x_a) < \varepsilon$ and the perturbation decays. Once the solar flux step change occurs at 200 ms, the averaged states become excited and $V(x_a) > \varepsilon$. This resets the amplitude of the perturbation to a_0 . Then, as $V(x_a) < \varepsilon$, the perturbation amplitude decays exponentially once again.

3.2.2. Comparative Analysis to Existing Methods

This section compares Lyap-ES to standard ES and a traditional MPPT technique: perturb & observe [2], [3] (P&O). Although some traditional MPPT methods are somewhat heuristic and may not appeal to the control

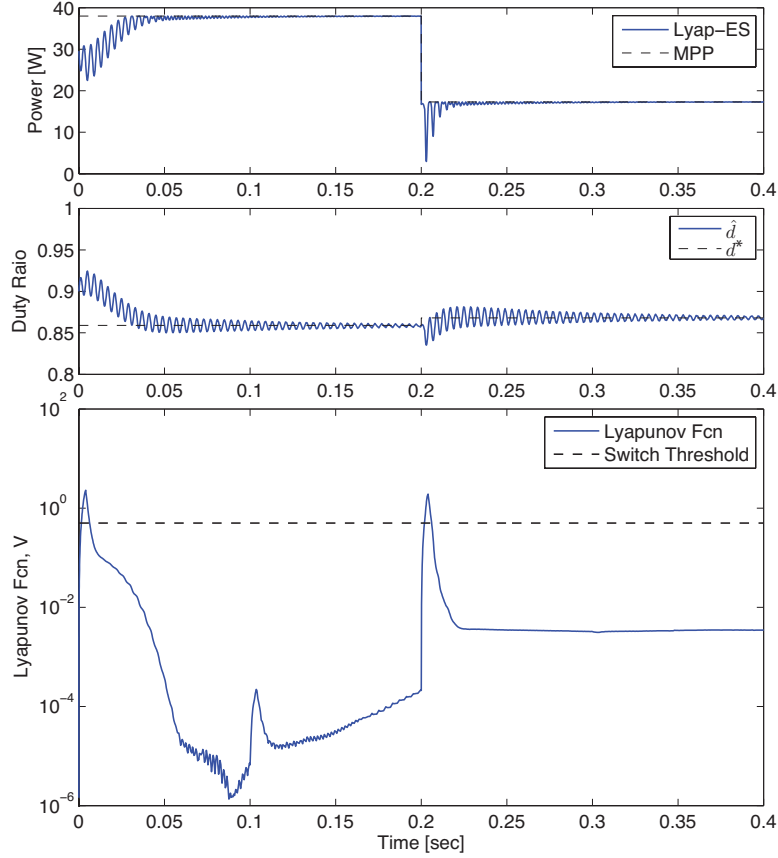


Figure 7: Time responses of PV array power, duty ratio, and Lyapunov function value for 1000 W/m^2 to 500 W/m^2 step change in solar irradiation.

theorist, they often produce satisfactory results and are simple to implement. However they lack guaranteed stability properties and have fundamental limitations. First we review the workhorse MPPT method, P&O.

Perturb & observe algorithms are the most widely used MPPT control systems, where the basic idea is as follows: Periodically perturb the PV array terminal voltage and measure the resulting power output. If output power increases, then perturb voltage in the same direction. If power output decreases, then reverse the perturbation. Note that when the MPP is reached, the P&O algorithm oscillates about this value, thus producing sub-optimal energy conversion efficiency. One may reduce the perturbation size

Table 1: Lyap-ES Controller Parameters.

Symbol	Description	Concept Demonstration Study	Experimental Data Study
u^0	Duty ratio for nominal MPP @ 1000W/m ² , 25°C	0.859	0.859
ω	Perturbation frequency	250 Hz	0.2 Hz
ω_h	High-pass filter cut-off freq.	50 Hz	0.04 Hz
ω_l	Low-pass filter cut-off freq.	50 Hz	0.04 Hz
a_0	Perturbation amplitude	0.015	0.01
k	Gradient update law gain	1	0.0008
ε	Lyap. Fcn. Threshold	0.01	20
γ	Perturbation amplitude decay rate	50	0.1
σ_P^2	Variance of measured power noise	0 W	0.2 W

to improve efficiency during steady-state, but this reduces convergence speed. Moreover, P&O cannot differentiate if a power increase is due to the voltage perturbation or a disturbance. An increase in solar irradiation or drop in temperature will confuse the P&O algorithm.

Figure 8 compares Lyap-ES to two benchmarks: P&O and basic ES (sinusoidal perturbation with no switching). The simulated conditions are identical to the previous subsection, however we do not consider varying incident solar irradiation. The perturbation amplitude and frequency of P&O are set equal to the Lyap-ES parameter values of a_0 and ω , respectively, to provide comparable results.

Several key observations arise from this study. First, ES and Lyap-ES are identical for the first 40ms. Afterwards, the switch condition is satisfied and Lyap-ES converges to u^* . Consequently, the power output from Lyap-ES upper-bounds the other algorithms. Secondly, although P&O converges faster than Lyap-ES, for the parameters considered here, the average output power is less than ES or Lyap-ES. Alternative parameter choices for ES and Lyap-ES can increase convergence speed (using the relations described in Remark 3), but may create bias induced from the high order harmonics that are insufficiently attenuated by the low pass filter. Ultimately, differences in convergence on the order of 10s of milliseconds are trivial compared

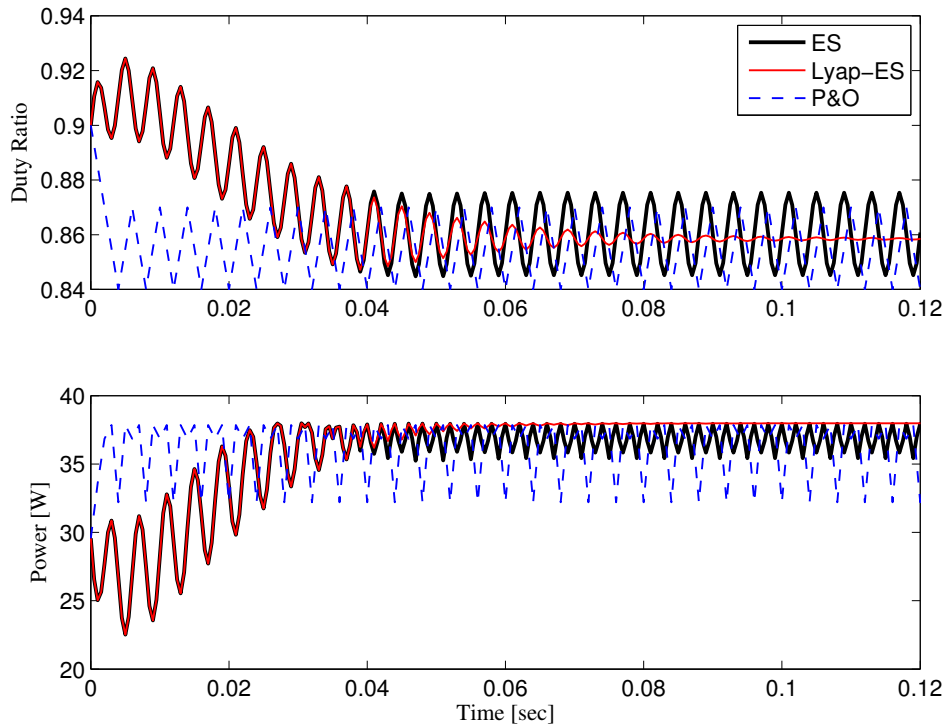


Figure 8: Comparison of Lyapunov-based switched extremum seeking (Lyap-ES) to basic extremum seeking (ES) and perturb & observe (P&O).

to the aggregate energy conversion over the hourly and diurnal time scales relevant to PV systems. Most importantly, ES and P&O oscillate about the MPP whereas Lyap-ES converges to it exactly, thus producing greater energy conversion rates. A comparison of power efficiencies is provided in Table 2.

3.3. Results with Experimental Data

In this section we test Lyap-ES with real-world solar irradiation and temperature data. A measurement and data logging device was fabricated to obtain real-world light and temperature data, shown in Figure 9. This autonomous device records ambient light and temperature and continuously logs the data onto a MicroSD storage card. Several data sets were recorded, over multiple days, in various locations across Southern California. For this study we cropped out a particularly transient data set with large swings

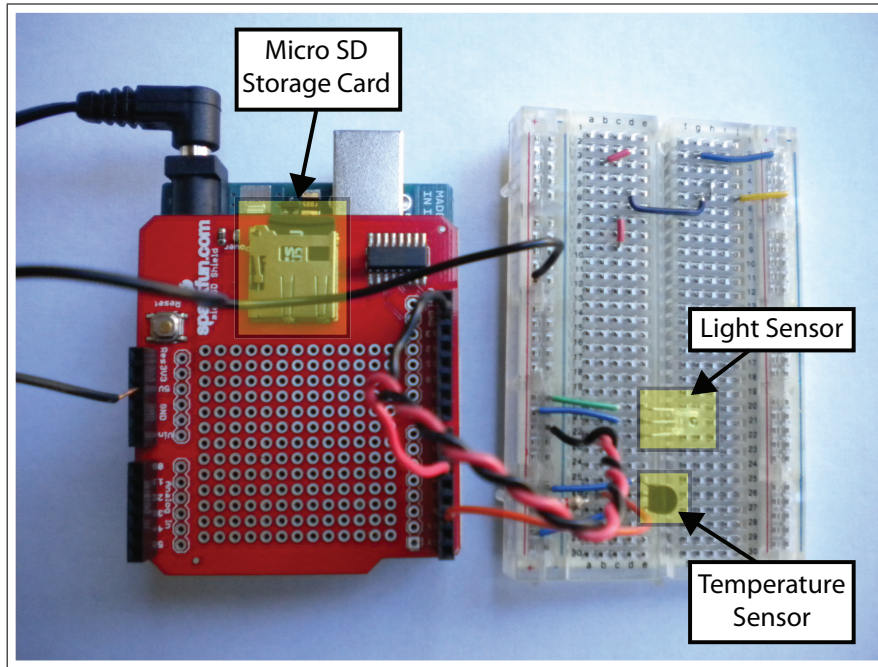


Figure 9: Data logger for measuring solar irradiation and ambient temperature

in temperature and solar irradiance to challenge Lyap-ES, as shown in Figure 10. Note that temperature and irradiance sensors are not required for Lyap-ES. The data logger in Fig. 9 is just used to obtain realistic disturbance data to test in simulation.

The highly transient measured solar irradiance and temperature data set was fed into the PV and DC/DC converter simulation models, controlled with Lyap-ES. Zero-mean, Gaussian noise with a variance of 0.2 W was added to the power measurement signal. Results are provided in Figure 10. The Lyap-ES controller parameters are provided in Table 1. Figure 10 demonstrates how the duty ratio input evolves as light and temperature change with time. When the environmental conditions do not change rapidly, the perturbation decays and the power output converges to the MPP. This point can be seen in the zoomed-in results provided in Figure 11, where the perturbation decays in the yellow shaded regions. Throughout the test, the Lyapunov function output repeatedly falls below and above the threshold, causing the perturbation to decay and re-enable, respectively. Under these environmental conditions, Lyap-ES converts the available power at 98.7% efficiency compared to 97.9%

Table 2: Power Efficiency Comparison

MPPT Method	P&O	ES	Lyap-ES
Power Efficiency, η $\eta = \int_0^T P(t)dt / \int_0^T P_{max}(t)dt$	0.952	0.946	0.970

for basic ES. Although this increase appears relatively small, it is free in the sense of only requiring changes to the MPPT controller firmware. Moreover, the algorithm has mathematically guaranteed stability and convergence properties.

3.4. Error between Nominal and Optimal MPP

Next we examine the impact of large errors between the nominal u^0 and optimal u^* MPPs. Recall that the Lyapunov function calculated in (28) measures the system's proximity to u^0 , measured in the coordinate system defined by (5)-(6). If $|u^0 - u^*|$ is sufficiently large, then the switching criterion $V(x_a) \leq \varepsilon$ may never be satisfied and the perturbation amplitude will not decay. Figure 12 demonstrates the Lyapunov function and power trajectories for various values of u^0 . In all cases except one ($u^0 = 0.85$) the switching criterion is not satisfied and the power oscillates around the true MPP. Under this worst-case scenario Lyap-ES degenerates into basic ES.

Degeneration of Lyap-ES into ES can be mitigated by appropriately selecting the threshold parameter ε and amplitude decay gain γ . That is, one may select ε sufficiently large and γ sufficiently small such that the algorithm enters the exponential decay mode quickly and the perturbation decays slowly. Figure 13 provides an example, where the threshold was raised to $\varepsilon = 0.5$ and the decay rate was lowered to $\gamma = 10$. Observe that the switching criterion is satisfied in all cases. Consequently, Lyap-ES converges and decays to the true MPP.

4. Conclusion

In this paper we propose a novel Lyapunov-based switched extremum seeking control method (Lyap-ES) that provides a practical extension to existing research on ES by eliminating limit cycles. Lyap-ES guarantees asymptotic convergence to the extremum of a static map by exponentially

decaying the perturbation once the algorithm reaches a neighborhood of the extremum. This neighborhood is approximated via Lyapunov stability analysis concepts that extend the stability proof originally presented in [13]. We apply Lyap-ES to the MPPT problem in a PV system as a case study to analyze performance. The advantage of Lyap-ES over traditional MPPT methods, e.g. P&O, is that the algorithm converges to the MPP asymptotically without entering a limit cycle. Moreover, the method is self-optimizing with respect to disturbances, such as varying solar irradiation and temperature shifts. We study Lyap-ES for MPPT in two steps. First, the concept is demonstrated by applying step changes in environmental conditions. Second, experimentally measured light and temperature data is applied to study Lyap-ES under realistic operating conditions. Future work will involve implementation into experimental photovoltaic systems. In summary, Lyap-ES offers a control-theoretic alternative for MPPT problems.

Appendix A. ES Control Parameter Selection

The synthesis process for an extremum seeking controller requires proper selection of the perturbation frequency ω , amplitude a_0 , gradient update law gain k , and filter cut-off frequencies ω_h and ω_l . The perturbation frequency must be slower than the slowest plant dynamics to ensure the plant appears as a static nonlinearity from the viewpoint of the ES feedback loop. Mathematically, this can be enforced by ensuring $\omega \ll \min\{\text{eig}(A)\}$, where A is the state matrix from linearizing the plant. Large values for a_0 and k allow faster convergence rates, but respectively increase oscillation amplitude and sensitivity to disturbances. More importantly, they can destroy stability. Therefore, one typically increases these parameter values to obtain maximum convergence speed for a permissible amount of oscillation and sensitivity. The filter cut-off frequencies must be designed in coordination with the perturbation frequency ω . Specifically, the high-pass filter must not attenuate the perturbation frequency, but the low-pass filter should - thus bounding the cut-off frequencies from above. Mathematically $\omega_h < \omega$ and $\omega_l < \omega$. Moreover, the filters should have sufficiently fast dynamics to respond quickly to perturbations in the control input, thereby bounding the cut-off frequencies from below. Generally, proper selection of the ES parameters is a tuning process [15]. However, the above guidelines are valuable for effective calibration.

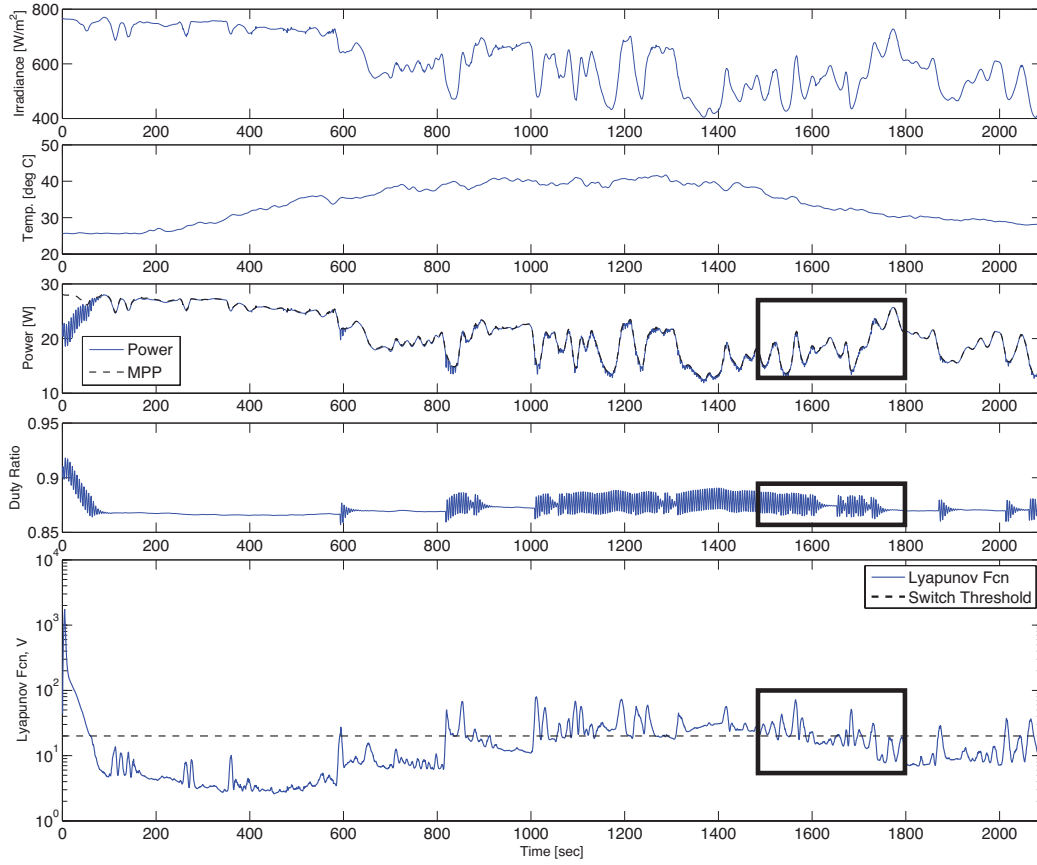


Figure 10: Evolution of solar irradiation, temperature, PV output power, DC/DC converter duty ratio, and the Lyapunov function value under the Lyap-ES control scheme. A zoom-in of the power and duty ratio outputs circumscribed by the rectangles are provided in Figure 11.

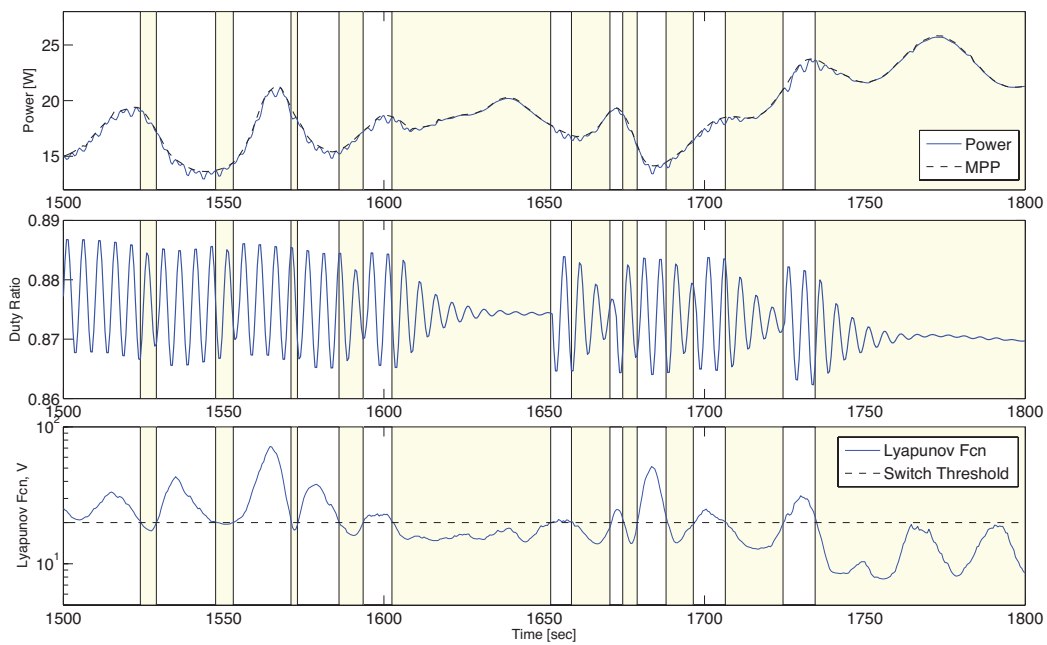


Figure 11: Zoom-in of PV output power, DC/DC converter duty ratio and Lyapunov function value from Fig. 10. The yellow and white shaded time-zones denote when the perturbation is decaying and re-enabled, respectively, as determined by the Lyapunov function/threshold crossing.

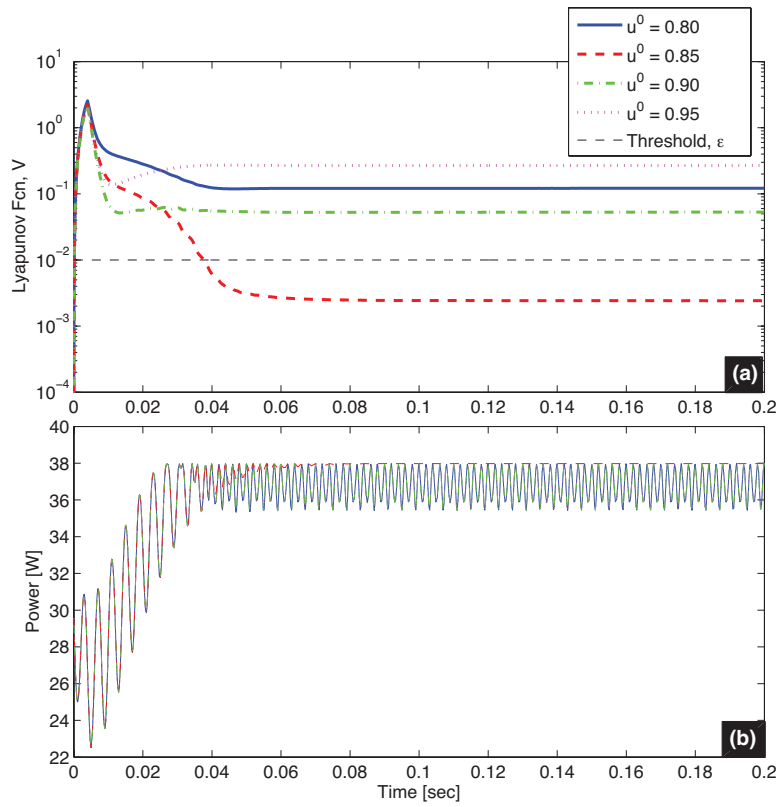


Figure 12: (a) Lyapunov function and (b) power trajectories for various nominal MPPs u^0 . The true MPP corresponds to $u^* = 0.859$. The switch criterion is satisfied for $u^0 = 0.85$ only.

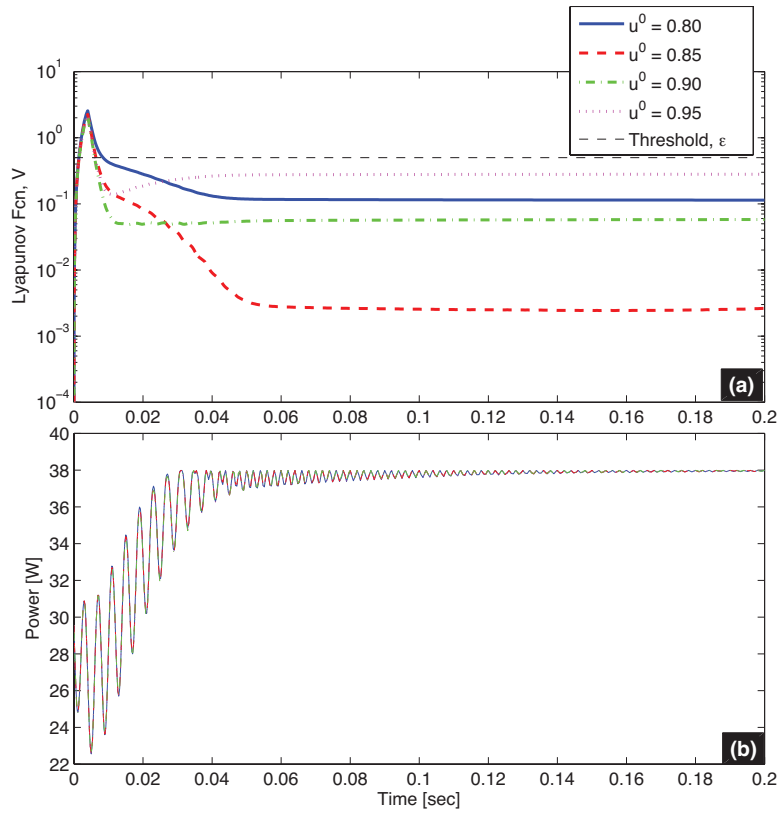


Figure 13: (a) Lyapunov function and (b) power trajectories for various nominal MPPs u^0 and adjusted parameters $\epsilon = 0.5$, $\gamma = 10$. The adjusted parameters compensate for errors between the nominal u^0 and true MPP $u^* = 0.859$.

References

- [1] T. Eswam, P. Chapman, Comparison of photovoltaic array maximum power point tracking techniques, *IEEE Transactions on Energy Conversion* 22 (2007) 439–449.
- [2] J. Kwon, B. Kwon, K. Nam, Three-phase photovoltaic system with three-level boosting MPPT control, *IEEE Transactions on Power Electronics* 23 (2008) 2319–2327.
- [3] N. Femia, G. Petrone, G. Spagnuolo, M. Vitelli, Optimization of perturb and observe maximum power point tracking method, *IEEE Transactions on Power Electronics* 20 (2005) 963–973.
- [4] V. T. Buyukdegirmenci, A. M. Bazzi, P. T. Krein, A comparative study of an exponential adaptive perturb and observe algorithm and ripple correlation control for real-time optimization, *2010 IEEE Workshop on Control and Modeling for Power Electronics* (2010).
- [5] K. Hussein, I. Muta, T. Hoshino, M. Osakada, Maximum photovoltaic power tracking: an algorithm for rapidly changing atmospheric conditions, *IEE Proceedings-Generation, Transmission and Distribution* 142 (1995) 59–64.
- [6] H. El Fadil, F. Giri, Climatic sensorless maximum power point tracking in pv generation systems, *Control Engineering Practice* 19 (2011) 513 – 521.
- [7] R. Leyva, C. Alonso, I. Queinnec, A. Cid-Pastor, D. Lagrange, L. Martinez-Salamero, Mpppt of photovoltaic systems using extremum - seeking control, *IEEE Transactions on Aerospace and Electronic Systems* 42 (2006) 249 – 258.
- [8] A. Bratcu, I. Munteanu, S. Bacha, B. Raison, Maximum power point tracking of grid-connected photovoltaic arrays by using extremum seeking control, *Journal of Control Engineering and Applied Informatics* 10 (2008) 3–12.
- [9] T. Eswam, J. W. Kimball, P. T. Krein, P. L. Chapman, P. Midya, Dynamic maximum power point tracking of photovoltaic arrays using ripple

- correlation control, *IEEE Transactions on Power Electronics* 21 (2006) 1282 – 1290.
- [10] D. Logue, P. Krein, Optimization of power electronic systems using ripple correlation control: A dynamic programming approach, *PESC Record - IEEE Annual Power Electronics Specialists Conference 2* (2001) 459 – 464.
 - [11] S. L. Brunton, C. W. Rowley, S. R. Kulkarni, C. Clarkson, Maximum power point tracking for photovoltaic optimization using ripple-based extremum seeking control, *IEEE Transactions on Power Electronics* 25 (2010) 2531 – 2540.
 - [12] A. M. Bazzi, P. T. Krein, Concerning maximum power point tracking for photovoltaic optimization using ripple-based extremum seeking control, *IEEE Transactions on Power Electronics* 26 (2011) 1611 – 1612.
 - [13] M. Krstic, H. Wang, Stability of extremum seeking feedback for general nonlinear dynamic systems, *Automatica* 36 (2000) 595–601.
 - [14] D. DeHaan, M. Guay, Extremum-seeking control of state-constrained nonlinear systems, *Automatica* 41 (2005) 1567–1574.
 - [15] Y. Chang, S. Moura, Air flow control in fuel cell systems: An extremum seeking approach, *Proceedings of the 2009 American Control Conference* (2009) 1052–1059.
 - [16] J. Creaby, Y. Li, S. Seem, Maximizing Wind Energy Capture via Extremum Seeking Control, *Proceedings of the 2008 ASME Dynamic Systems and Control Conference* (2008) 361–387.
 - [17] K. Ariyur, M. Krstić, *Real-time optimization by extremum-seeking control*, Wiley-Blackwell, 2003.
 - [18] M. Krstić, Performance improvement and limitations in extremum seeking control, *Systems & Control Letters* 39 (2000) 313–326.
 - [19] Y. Tan, D. Nešić, I. Mareels, On the choice of dither in extremum seeking systems: A case study, *Automatica* 44 (2008) 1446–1450.

- [20] D. Nešić, Y. Tan, W. Moase, C. Manzie, A unifying approach to extremum seeking: Adaptive schemes based on estimation of derivatives, *Proceedings of the IEEE Conference on Decision and Control* (2010) 4625–4630.
- [21] S. Moura, Y. Chang, Asymptotic convergence through lyapunov-based switching in extremum seeking with application to photovoltaic systems, *Proceedings of the 2010 American Control Conference* (2010) 3542–3548.
- [22] A. Ghaffari, M. Krstić, D. Nesic, Multivariable Newton-based extremum seeking, *Proceedings of the IEEE Conference on Decision and Control* (2011) 4436–4441.
- [23] H. Khalil, *Nonlinear systems*, volume 3, Prentice hall, 1992.
- [24] S. Bull, Renewable energy today and tomorrow, *Proceedings of the IEEE* 89 (2001) 1216 –1226.
- [25] G. Vachtsevanos, K. Kalaitzakis, A hybrid photovoltaic simulator for utility interactive studies, *IEEE Transactions on Energy Conversion* (1987) 227–231.
- [26] G. Masters, *Renewable and efficient electric power systems*, Wiley Online Library, 2004.
- [27] D. Chan, J. Phang, Analytical methods for the extraction of solar-cell single-and double-diode model parameters from iv characteristics, *IEEE Transactions on Electron Devices* 34 (1987) 286–293.
- [28] J. Gow, C. Manning, Development of a photovoltaic array model for use in power-electronics simulation studies, in: *IEE Proceedings-Electric Power Applications*, volume 146, IET, pp. 193–200.
- [29] M. Villalva, J. Gazoli, et al., Comprehensive approach to modeling and simulation of photovoltaic arrays, *Power Electronics, IEEE Transactions on* 24 (2009) 1198–1208.
- [30] S. R. Sanders, J. Noworolski, X. Z. Liu, G. C. Verghese, Generalized averaging method for power conversion circuits, *IEEE Transactions on Power Electronics* 6 (1991) 251 – 259.